International Journal of Pharmaceutics 544 (2018) 425–432

Contents lists available at ScienceDirect

International Journal of Pharmaceutics

journal homepage: www.elsevier.com/locate/ijpharm

3D printed microneedles for insulin skin delivery

Cristiane Patricia Pissinato Pere[a], Sophia N. Economidou[a], Gurprit Lall[a], Clémentine Ziraud[c], Joshua S. Boateng[b], Bruce D. Alexander[b], Dimitrios A. Lamprou[a], Dennis Douroumis[b,*]

[a] Medway School of Pharmacy, University of Kent, Medway Campus, Central Avenue, Chatham Maritime, Chatham, Kent ME4 4TB, United Kingdom
[b] Faculty of Engineering & Sciences, University of Greenwich, Medway Campus, Central Avenue, Chatham Maritime, Chatham, Kent ME4 4TB, United Kingdom
[c] Polytech Marseille Filière Matériaux, Luminy Case 925, 13288 Marseille Cedex 09, France

ARTICLE INFO

Keywords:
3D printing
Microneedles
Inkjet coating
Insulin

ABSTRACT

In this study, polymeric microneedle patches were fabricated by stereolithography, a 3D printing technique, for the transdermal delivery of insulin. A biocompatible resin was photopolymerized to build pyramid and cone microneedle designs followed by inkjet print coating of insulin formulations. Trehalose, mannitol and xylitol were used as drug carriers with the aim to preserve insulin integrity and stability but also to facilitate rapid release rates. Circular dichroism and Raman analysis demonstrated that all carriers maintained the native form of insulin, with xylitol presenting the best performance. Franz cell release studies were used for *in vitro* determination of insulin release rates in porcine skin. Insulin was released rapidly within 30 min irrespectively of the microneedle design. 3D printing was proved an effective technology for the fabrication of biocompatible and scalable microneedle patches.

1. Introduction

Over the last 20 years transdermal microneedles (MNs) have paved the way for the delivery of various active substances across the skin (Alkilani et al., 2015; Sanjay et al., 2017). These miniature devices are used for the administration of active drug substances and vaccines, including genetic material such as RNA and DNA (Chen et al., 2016). MNs can pierce the skin in a painless way and through the penetration of the stratum corneum the drug substance is released into the dermis. The minimally invasive administration of MNs has shown to improve systemic drug adsorption and thus bioavailability (Wermeling et al., 2008). Ideally, they provide improved patient compliance as they do not stimulate nerves associated with pain and can be self-administrated (Kaushik et al., 2001). MNs are classified into four categories including solid, coated, hollow, hydrogel – forming and dissolvable microneedles usually made of metal, polysaccharides or polymeric materials (Ita, 2015).

Recent advances in skin delivery mediated by MNs involve the development of polyvinylpyrrolidone (PVP) and trehalose dissolvable MNs for the encapsulation of peptides. The MNs achieved rapid systemic delivery by dissolving in the interstitial fluid of the skin and retained the antimicrobial activity of the peptide (Dillon et al., 2017). In another study, MNs made of chitosan and beta-sodium glycerophosphate showed efficient delivery of levonorgestrel in vivo without causing any skin irritation. The pharmacokinetic profile of the drug, presented similarities with the respective one of oral suspension, demonstrating that drug-loaded dissolving MN systems are an appealing alternative to traditional levonorgestrel administration routes (Yao et al., 2017). In another study, MNs were coated with 60 μg of a plasmid DNA cocktail encoding the Leishmania infantum nucleosomal histones H2A, H2B, H3 and H4 and their immunization capacity was compared against subcutaneous or intradermal injection of the plasmid. The results demonstrated that MNs improved immunogenicity, but higher plasmid doses might be required for better Leishmania control (Moreno et al., 2017).

Significant efforts have been made in the skin delivery of insulin analogs by using MNs in order to address the accuracy of the injections, decrease leakage of insulin to the skin surface, and reduce pain caused by repeated injections (Guo and Wang, 2017; Narayan, 2014). In a recent study, MNs for insulin delivery, composed of modified alginate and hyaluronate, were fabricated by micromoulding (Yu et al., 2017). The optimized MNs showed good mechanical strength and piercing capacity while insulin bioactivity was not affected. In vivo studies demonstrated a sustained hypoglycaemic effect with high relative pharmacologic availability and relative bioavailability, compared to subcutaneous injections. Clinical studies in diabetic Sprague – Dawley rats demonstrated effective hypoglycaemic control when insulin was released from calcium sulfate and gelatine biodegradable composite microneedle patches, showing that insulin is a suitable candidate for MN-mediated transdermal delivery (Yu et al., 2017).

* Corresponding author.
E-mail address: D.Douroumis@gre.ac.uk (D. Douroumis).

https://doi.org/10.1016/j.ijpharm.2018.03.031
Received 23 November 2017; Received in revised form 20 February 2018; Accepted 15 March 2018
Available online 16 March 2018
0378-5173/

However, there are several pitfalls in MN skin delivery, related to the manufacturing process and materials used for the development of MN patches. Micromoulding is the most common approach used for the fabrication of dissolving and gel - forming MNs and involves a sequence of time-consuming and difficult to scale-up steps. On the other hand, coating technologies do not always result in uniform, accurate and reproducible active coated layers and fail to avoid drug deposition on the MNs substrate. There are also serious concerns regarding the biocompatibility, skin irritation and even sterilization issues (McCrudden et al., 2015) of the materials (e.g. silicon, polymers) used for MNs fabrication as most of them are suitable for oral use but not approved for skin delivery. The limited loading of active substances in most of these MN technologies is another shortcoming for efficient transdermal delivery. More explicitly, coating techniques limit the drug amount that can be loaded in the system to 1 mg maximum (Kim et al., 2012) while larger amounts (up to 33 mg) have been successfully delivered by dissolving MNs (McCrudden et al., 2014).

3D printing or additive manufacturing is a family of technologies that employ a virtual Computer Aided Design (CAD) model to create a physical object through the consecutive creation of layers. It was launched in 1980s (Kodama, 1981; Hull, 1984) and it has revolutionized the field of pharmaceutical, biomedical and material sciences due to the capabilities for rapid and cost-effective prototyping of complex structures (Pedde et al., 2017). 3D printing endows the prototyping and fabrication process with versatility; objects are manufactured in a one-step fashion with high degrees of complexity and reproducibility.

Among the various technologies that comprise 3D printing, photopolymerisation-based techniques enable the fabrication of structures through the consecutive layer-wise polymerization of UV-sensitive polymers, through a curing process named photopolymerization. Stereolithography (SLA), Digital Light Processing (DLP) and Two-Photon-Polymerization (2PP) are among these technologies (Economidou et al., 2018). In the field of Transdermal Drug Delivery (TDD), Gittard et al. employed a photopolymerisation-based printer (DLP) to fabricate MNs of various geometries for wound healing applications, followed by pulse laser deposition of silver and zinc oxide thin films (Gittard et al., 2011). Similarly, Lu et al. incorporated Dacarbazine (1–2%), a skin anticancer drug, into poly(propylene fumarate)/drug blends followed by photopolymerization through a microstereolithographic (DLP) apparatus that built the MN arrays (Lu et al., 2015).

In this study, we employed SLA to fabricate MN arrays of different designs followed by inkjet printing of insulin – sugar films. 3D printed patches, featuring MN with cone and pyramid geometries, were made using a Class 1 biocompatible resin with excellent mechanical strength and piercing capacity. Mannitol, trehalose and xylitol, were used as insulin carriers in order to preserve insulin activity prior to the application of uniform and accurate “active” coating on the MN surface.

2. Materials and methods

Insulin solution from bovine pancreas (10 mg mL^{-1}) and trehalose dihydrate were purchased from Sigma-Aldrich (Gillingham, UK), while Xylisorb® 90 (Xylitol) and Pearlitol® (mannitol) were kindly donated by Roquette Freres (France). The printing polymer was the biocompatible Class I resin, Dental SG, procured by Formlabs. All solvents were of analytical grades.

2.1. 3D printing of microneedles

Two different MN designs, pyramid and cone, were developed using appropriate engineering software (SolidWorks by Dassault Systems), featuring square and circular cross-sections, respectively. The length of all MNs was 1 mm while the dimensions of the base cross-sections were 1 × 1 mm for the pyramid and ø 1 mm for the cone. The MNs were built as attached to a solid 15 × 15 × 1 mm substrate, forming patches of 48 MNs each. The arrays were fabricated using a Form 2 stereolithography (SLA) printer by Formlabs, with high resolution capabilities (25 and 140 μm for z and x axes, respectively). To obtain higher mechanical properties, the MN arrays, after being washed in isopropyl alcohol to remove excess resin, were cured under ultraviolet radiation for 60 min at 40 °C (MeccatroniCore BB Cure Dental station).

2.2. Inkjet printing of insulin formulations microneedles

The insulin solutions were printed onto each MN surface in the form of fine droplets using an inkjet printer (NanoPlotter II, Gesim, Germany) through a piezo-driven dispenser (PicPip 300). All MN arrays were positioned at 45° relative to the dispenser and for each coating cycle, 10 dots of 2 droplets of a coating formulation were dispensed longitudinally to the axis of each MN. The process was repeated for 46 jetting cycles resulting in 10 UI (350 μg) of insulin per array. Solvent (de-ionised water) was evaporated to produce uniform and reproducible solid thin films on the MNs after 24 h of incubation at room temperature. For the purposes of this study three coating formulations were used, consisting of insulin:xylitol (5:1 wt/wt), insulin: mannitol (5:1 wt/wt) and insulin:trehalose (5:1 wt/wt) as 2% solid content.

2.3. Scanning electron microscopy (SEM)

The MN arrays were mounted onto aluminium stubs using a double-sided carbon adhesive tape (Agar scientific, UK). Each MN array was examined by SEM (Hitachi SU 8030, Japan) using a low accelerating voltage (1.0 kV). A low accelerating voltage was used to avoid electrical charges on the MNs. The images of the MNs were captured digitally from a fixed working distance (11.6 mm) using different magnifications (30, 80, 110 or 120×).

2.4. Circular Dicroism (CD) analysis

The formulations were diluted to 1.0 mg mL^{-1} in deionized water and the spectra were recorded at 20 °C between 190 and 260 nm by CD (Chirascan, Applied Photophysics, UK) using a 0.1 mm polarization certified quartz cell (Hellma). Spectra were recorded using a step size of 1 nm, a bandwidth of 1 nm and an acquisition time of 1 s. Four scans were recorded for each sample, averaged and a corresponding spectrum of water was subtracted from each spectrum. For estimation of the secondary structural composition of insulin, the CD spectra were evaluated using CDSSTR method (Sreerama and Woody, 2000).

2.5. Raman analysis

The films of the formulations and their respective components were analysed using Raman spectroscopy (Jobin Yvon LabRam I) with a laser of 532 nm wavelength coupled with an optical microscope with 50× objective.

2.6. Penetration of MN in porcine skin

The necessary force required to pierce the skin has been found to be straightforwardly affected by the geometry of the MNs (Davis et al., 2004). In this study, to determine the effect of needle shape on the force required for skin penetration, piercing tests using porcine skin were conducted. In order to have a frame of reference with respective literature, metallic MN arrays were tested as well, the fabrication and physical characteristics of which, are described elsewhere (Ross et al., 2015). A texture analyser was employed, and the MN array was mounted on the moving probe using double-sided adhesive tape. Prior to testing, the porcine skin samples were placed in waxed petri dishes. Continuous force and displacement measurements were recorded to identify the point of needle insertion. The speed of the moving probe was 0.01 mm/s.

2.7. Skin preparation for in-vitro MN testing

Full thickness abdominal porcine skin was collected from a local slaughterhouse (Forge Farm Ltd, Kent, UK). The abdominal hair was shaved using a razor blade. The collected skin was stored at 4 °C until it was used. The fatty tissue below the abdominal area of porcine skin was removed with a scalpel and then pinned onto polystyrene block and wiped with 70% ethanol. The skin was then cut at 750 µm by applying the dermatome at an angle of ± 45° (Padgett dermatome, Integra LifeTMSciences Corporation USA). The thickness of the skin was measured by using a calliper and the tissue disks of the required dimensions were cut for the Franz diffusion cells using a scalpel. The skin tissue was placed onto filter paper soaked in a small amount of saline phosphate buffer (pH 7.4) for 2 h.

2.8. In vitro release of insulin coated MNs

Release studies of insulin were undertaken in abdominal porcine skin using Franz diffusion cells (PermeGear, Inc., PA, USA). Skin samples with a total diffusion area of 1.1 cm^2 were then placed in phosphate buffered saline (PBS; pH 7.4) for 1 h before the *in vitro* studies. The MN arrays were inserted into the abdominal porcine skin samples for 30 s using manual finger pressure. A skin pierced MN array was mounted onto the donor compartment of a Franz diffusion cell. The temperature of the Franz cells was maintained at 37 °C using an automated water bath (Thermo Fisher Scientific, Newington, USA). Sample fractions (6–6.5 mL/h) were collected using an auto-sampler (FC 204 fraction collector, Gilson, USA) attached to the Franz diffusion cells. Statistical analysis for the drug release was performed by using a Mann-Whitney nonparametric test (InStat, GraphPad Software Inc., San Diego, CA, USA), where samples are considered to be statistically significant at $p < 0.05$.

2.9. HPLC analysis

The amount of insulin collected from the receptor fluid was determined by High-Performance Liquid Chromatography (HPLC; Agilent Technologies, 1200 series, Cheshire, UK) equipped with a Phenomenex Jupiter 5u c18 300 Å, LC Column (250 × 4.60 mm, particle size 5 µm, Macclesfield, UK). The mobile phase consisted of water with 0.1% TFA and acetonitrile with 0.1% TFA (66:34v/v), with a 1 mL min^{-1} flow rate. The column was equilibrated at 35 °C, the injection volume was 20 µL and the eluent was analysed with a UV detector at 214 nm. The results were integrated using Chemstation® software and the samples analysed in triplicates.

3. Results and discussion

MN arrays with cone- and pyramid-shaped needles were successfully printed using an additive manufacturing technique known as stereolithography. The SLA processes a Class I biocompatible resin to build up structures in a layer – by – layer manner from CAD models. Dental SG resin is one of the few commercially available, biocompatible, FDA certified polymers that are compatible with stereolithography printers and the only Class I compatible with the Form 2 system. After printing, the MN arrays were cured using a light source – UV laser to harden the plastic MN patches through a photopolymerization process resulting in improved mechanical properties. As shown in Fig. 1 SLA produced two different designs of pyramid (6 × 8) and cone-shaped (6 × 8) MN patches with 1000 µm height, 1000 µm width and 1.85 mm interspacing distance (measured from tip-to-tip). In Fig. 1a and b the build layers of both MN designs appear highly consistent and reproducible. The high resolution of the printer permitted the reproducible fabrication of arrays in excellent detail, leading to the formation of sharp needle tips that favour the skin insertion. The low cost of the printing material and the fast production speed renders SLA

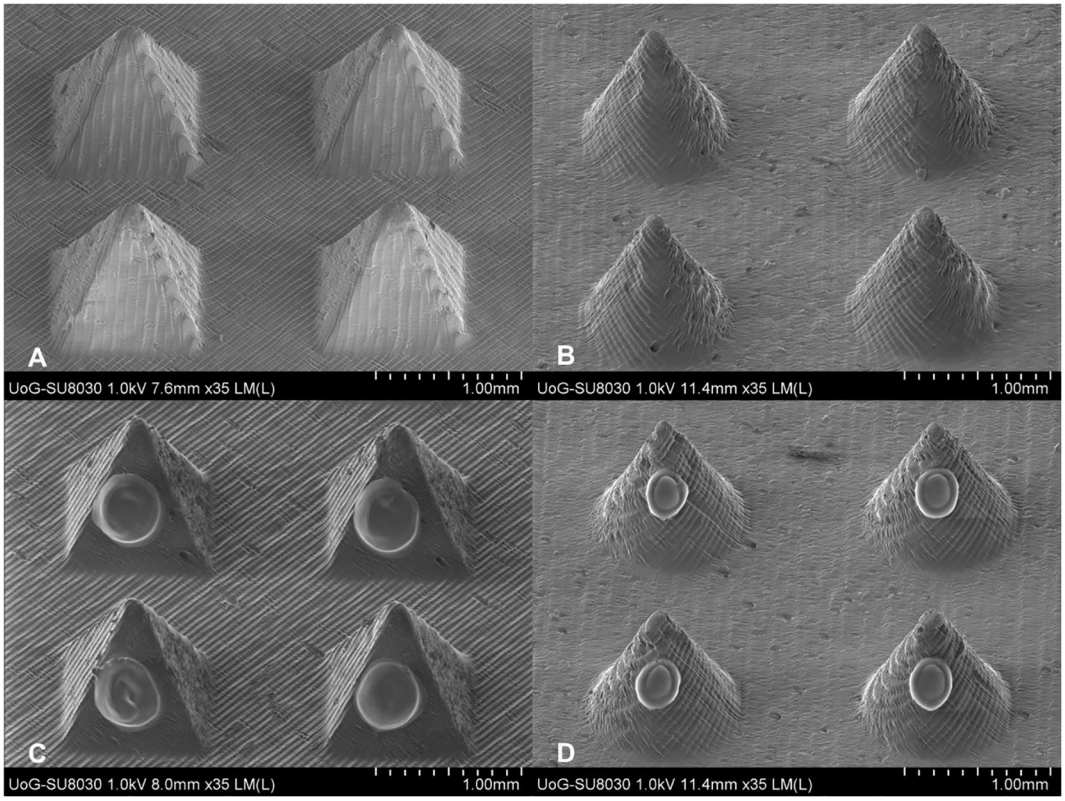

Fig. 1. SEM images of 3D printed microneedle designs of: a) plain pyramid, b) plain cone, c) insulin coated pyramid and c) insulin coated cone.

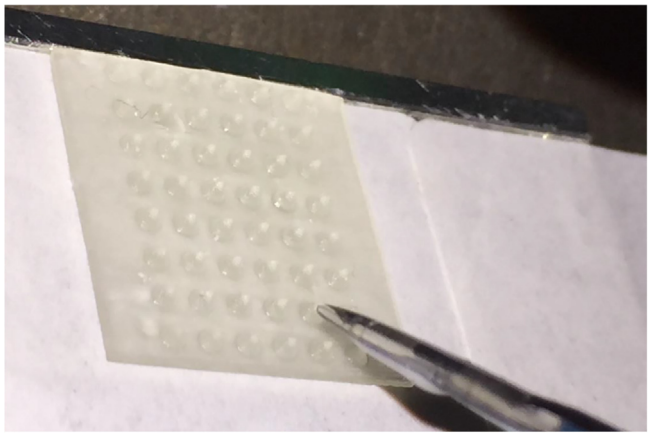

Fig. 2. Inkjet coating process of 3D printed microneedles.

an attractive process for MN fabrication. Quantitively, the currently available commercial SLA apparatuses have a limited print volume and the existing print volume (145 × 145 × 175 mm) allows the manufacturing of up to 49 MN arrays within 2 h according to the dimensions and methodology described. Upscaling of the process at a manufacturing scale depends on the introduction of printers with larger print volumes. However, considering the low cost of these printers and the short fabrication time, parallel printings in multiple printers can generate a great number of arrays fast and accurately.

Inkjet printing was then employed to apply coatings of insulin and sugar solutions through a piezoelectric dispenser. This 2D printing approach has been previously used for coating of metal MNs (Ross et al., 2015; Uddin et al., 2015) where by optimizing the applied voltage (mV) and the pulse duration (ms) droplets of 300 pL volume with consistent particle size of 100–110 µm as observed by the printer's stroboscope, were produced. The dispenser's tip (50 µm) was kept close to the microneedle surface to avoid losses of the coating material (Fig. 2). Fig. 1c and d shows the morphologically excellent coatings on the MN surface without the presence of any satellite droplets on the substrate. In addition, the inkjet printing led to the formation of uniform layers with high precision and reproducibility without the creation of bulky coatings observed in conventional techniques such as dip coating.

The coating formulations consisted of insulin solutions of two alcohol sugars (xylitol, mannitol) and a disaccharide (trehalose) specifically selected as drug carries. The selection of those excipients was twofold, firstly because they favour and enhance insulin stability in solid state and secondly, we anticipated a rapid coating dissolution immediately after the MN piercing (Yong et al., 2009; Kim et al., 2009; Schiffter et al., 2010).

3.1. Circular dichroism

Circular dichroism (CD) is a well-known spectroscopic technique used to study the secondary structure of proteins and polypeptides in a solution. In order to investigate the effect of different sugars on the structure of insulin, CD experiments were carried out. The secondary structure of insulin in all samples was also estimated by the CDSSTR method (Sreerama and Woody, 2000) and it is quantitatively summarized in Table 1.

In Fig. 3 all far-UV CD spectra of insulin and insulin-sugar formulations showed two negative minima around 210 and 225 nm, commonly associated with predominant features of α-helices structure which is in close agreement with the spectra already reported in literature (Ettinger and Timasheff, 1971; Sarmento et al., 2007; Yong et al., 2009; Andrade et al., 2015). Also, the secondary structure of pure insulin in solution estimated by CDSSTR method, agrees well with that obtained by others (Melberg and Johnson 1990; Yong et al. 2009). The spectra of insulin-mannitol and insulin-trehalose show a slight decrease in the absolute intensities at 210 and 225 nm which can indicate

Table 1
Secondary structure prediction by CDSSTR using far-ultraviolet CD spectra.

	Insulin	Insulin:Xylitol 5:1	Insulin:Mannitol 5:1	Insulin:Trehalose 5:1
Alpha Helix	58%	57%	54%	53%
β-Sheet	7%	7%	10%	10%
Turn	10%	11%	11%	11%
Random coil	26%	26%	26%	26%

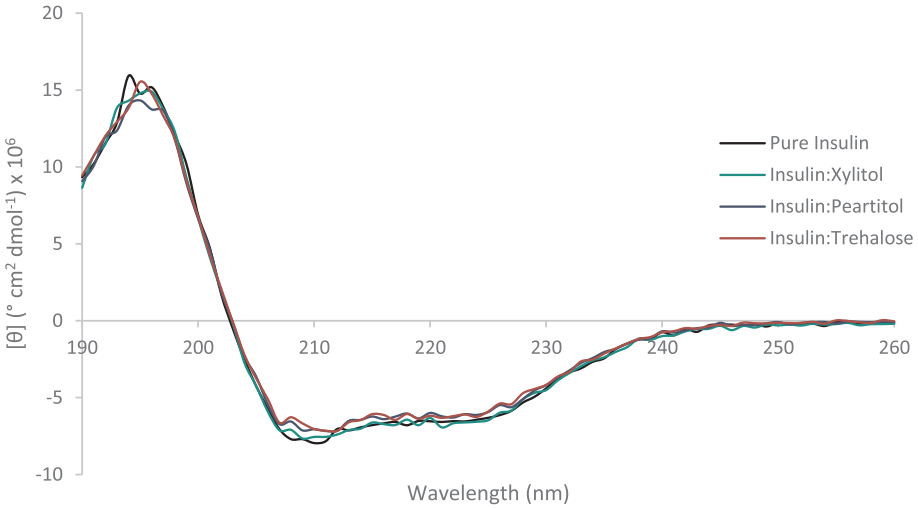

Fig. 3. CD of insulin and insulin formulations.

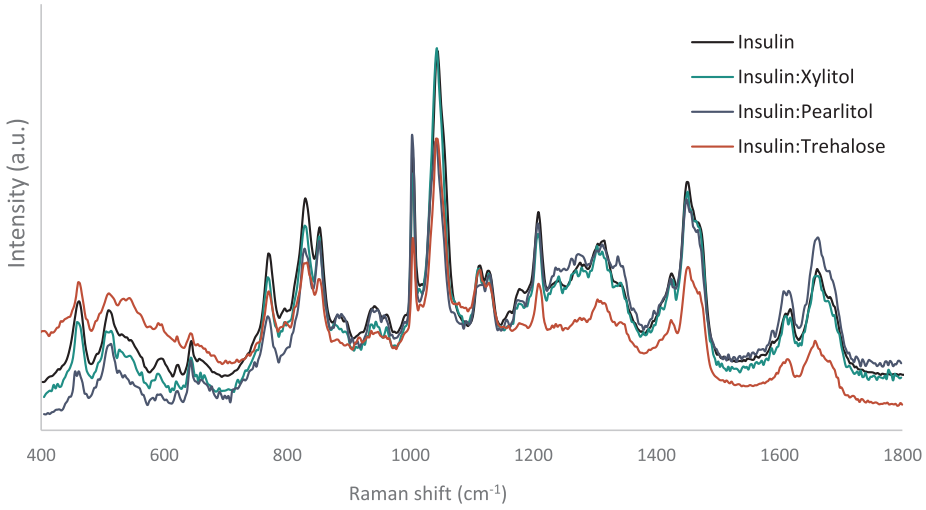

Fig. 4. Raman spectra from 400 to 1800 cm^{-1} of pure insulin and insulin formulations.

changes in the ratio of α-helix and β-sheet content. According to the secondary structure estimation, these changes do indicate a decrease in α-helix content of 4 and 5% for mannitol and trehalose formulations, respectively, with a simultaneously increase of 4% in the β-sheet. Although, similar effect of trehalose on α-helix content was reported by Yong et al. (2009), the reason for this is still unclear and further research is needed.

Among the tested sugars, xylitol presented the best capability to maintain insulin in its native form with almost the same amount of α-helix content. Regarding the stability and storage requirements, insulin coated MN arrays where placed for stability studies at 2–8 °C for 30 days. The stored samples were further examined by CD and no changes on the spectra where observed compared to the freshly coated MNs (data not shown). These findings suggest that coating formulations provide efficient insulin protection according to regulatory requirements.

3.2. Raman spectroscopy

Raman spectroscopy has been widely used to study possible changes in chemical composition as well to study important information about protein conformation.

In this study, the spectrum of native insulin, Fig. 4, shows a strong amide I band at 1661 cm^{-1} and a shoulder near 1682 cm^{-1} (CO stretching with some contribution from the stretching of CN groups and CCN deformations) which are indicative of α-helix structure and random coil form, respectively, being in accordance with Yu et al. (1972).

All insulin formulations spectra display a similar band shape to the native insulin, assigning the α-helix structure. However, insulin-xylitol and insulin-mannitol formulation display a shift towards greater frequency, 1663 cm^{-1} and 1662 cm^{-1}, respectively, and insulin-trehalose was shifted to lower frequency, at 1658 cm^{-1}. Furthermore, for mannitol formulation, an increase in the amide I peak absorbance was seen, while a pronounced decrease was noted for the trehalose one. Those changes might be due to the different effect of each sugar on the vibrational spectra of insulin as well as on the intra- and inter-chain couplings between the adjacent peptide units as stated by Carpenter and Crowe (1989) and Souillac et al. (2002).

Characteristic peaks of sugars were not found in Raman spectra due to the fact that insulin is more concentrated in the formulation films compared to the carbohydrate films. X-ray diffraction (XRD) analysis (data not shown) suggested that the sugars were amorphous and therefore it is likely to present a weak Raman spectrum. It has also been suggested that there is also hydrogen bond between the sugar and the dried protein as reported by Carpenter and Crowe (1989). This interaction is known as water-replacement mechanism and it is responsible for preventing protein denaturation (Timasheff, 1993) by replacing water molecules with other hydrogen bond reducing then the probability of protein aggregation during the drying process (Souillac et al., 2002). Therefore, the developed formulations have good capability to maintain insulin molecule in its native form with high amounts of α-helix content which is essential for its biological activity.

3.3. Penetration of MN in porcine skin

The polymeric arrays featuring different MN shapes along with the metallic ones were inserted in porcine skin samples using a texture analyser. All MN designs successfully pierced the skin and no MN failure was reported. Force against displacement data were continuously recorded throughout the penetration and the data are shown in Fig. 5.

The sharp drop of the load corresponds to the insertion of the MN into the skin (Davis et al., 2004). Prior to that event, all curves present an initial linear portion (displacement < 0.3 mm). The slope then change constantly as the MN continues to penetrate the skin revealing a non-linear connection between the developed forces and the penetration depth.

This behaviour could be attributed to the viscoelastic nature of the skin tissue, however indentation studies by Pailler-Mattei et al. (2008) proposed the neglecting of the viscous part and the consideration of the skin as an elastic material in the load range of 0–20 N. Considering that all the measurements are well below the 20 N margin, a linear connection between force and displacement throughout the test should be expected. The divergence from linearity shows that the needle penetration of the skin starts earlier than the sharp drop of load. The load increases as the needle goes deeper through the skin until a threshold force is reached and insertion becomes abrupt. These findings are in accordance with the work from Gittard et al. (2013) that concluded that MN penetration should be viewed as a series of sequential penetrations until a

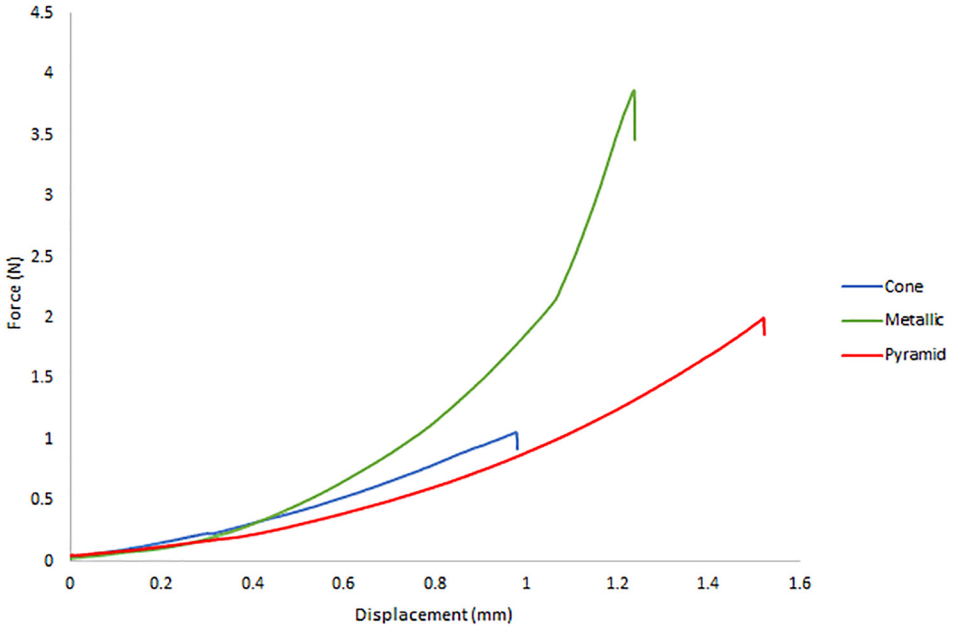

Fig. 5. Force *vs* displacement curves for MN penetration in porcine skin.

maximum force is applied, rather than a single event. The threshold load indicates that the MN insertion is successful, and the respective values are depicted in Fig. 6.

Regarding the different designs and apart from the metallic MN that require the maximum threshold force for penetration, the cone design requires the least force to penetrate the porcine skin. Since both designs are dimensionally similar, the variation of the maximum load required for penetration can be attributed to the difference of the MN-to-skin contact area between the two designs. Indeed, Eq. (1) yields a total contact surface for the cone design, of 1.76 mm^2 per needle. On the other hand, the lateral surface for pyramid is found to be 2.24 mm^2 per needle, from Eq. (2).

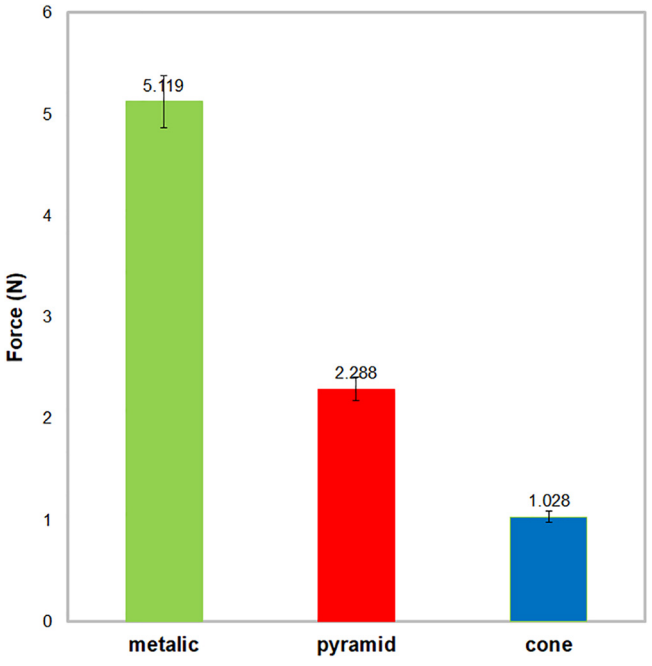

Fig. 6. Maximum forces for MN penetration in porcine skin.

$$S_{cone} = \pi r\sqrt{h^2 + r^2} \quad (1)$$

where: r is the base radius and h the height of the MN.

$$S_{pyramid} = l\sqrt{\frac{w^2}{2} + h^2} + w\sqrt{\frac{l^2}{2} + h^2} \quad (2)$$

where: l is the length of the base, w the width of the base, and h the height of the MN.

The 21% difference in area between the two designs indicates that the frictional forces after initial penetration until the threshold force in reached, are greater for the pyramid needles. As a result, greater loads are required to achieve further penetration through the skin.

3.4. Insulin release studies

In vitro insulin release studies were conducted using dermatomed porcine skin through Franz diffusion cells. The alcohol sugars (mannitol, xylitol) and the disaccharide sugar (trehalose) provided excellent coatings on the MN surface and due to their hydrophilic nature were expected to provide rapid release rates. Indeed, as shown in Fig. 7a and b the observed insulin release rates in the first 2 min varied from 63 to 69% and from 57 to 64% for the pyramid and cone-shaped 3D microneedles, respectively. After 20 min more than 80% of insulin was detected in the receptor's compartment and 90–95% in 30 min. Furthermore, the release profiles were almost identical for all carriers and no statistical difference was observed for each MN design (two-tail $p = 0.0026$). The rapid insulin profiles were attributed to the extremely high hydration rates of the alcohol sugars and the disaccharide respectively, that take place within the porcine skin micro-cavities created upon the MN piercing.

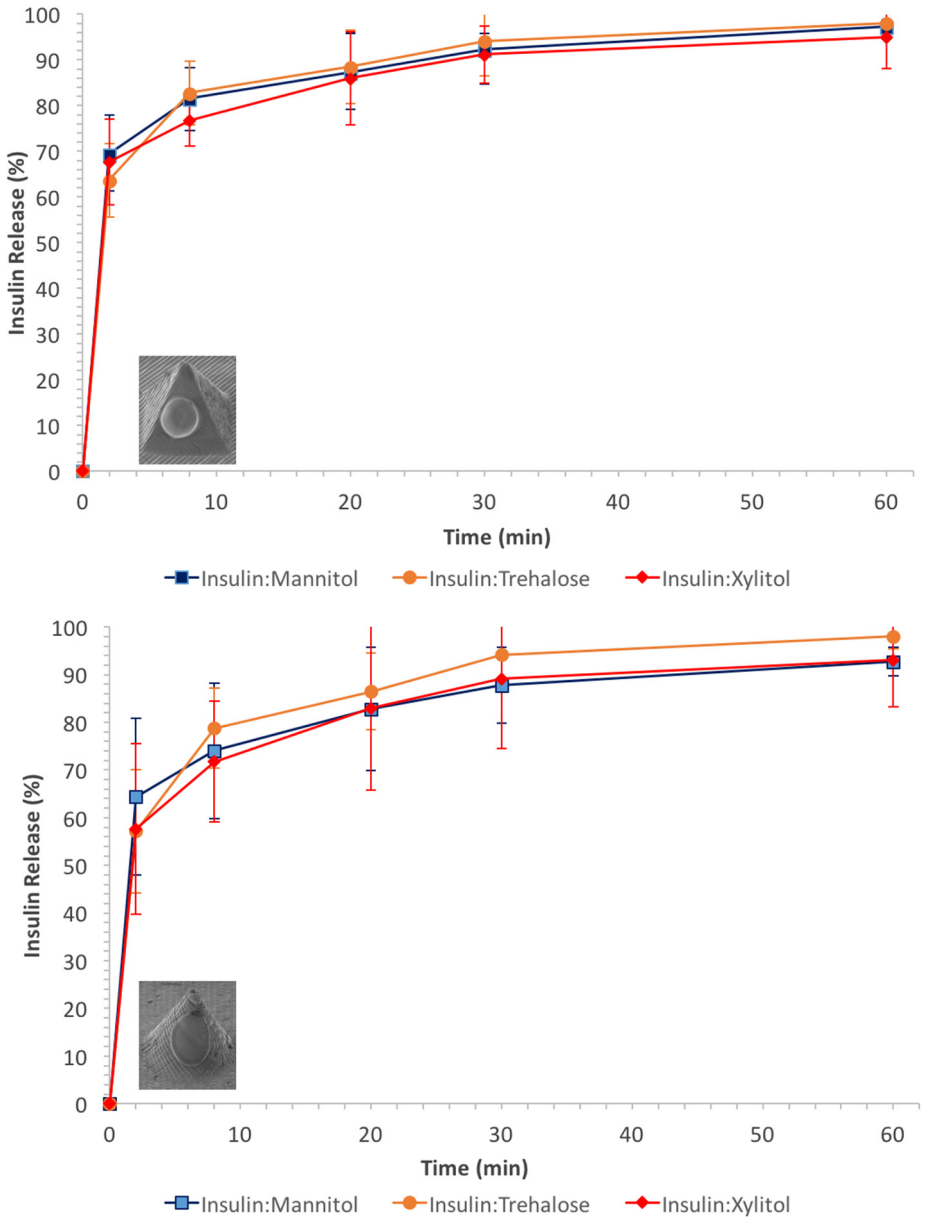

Fig. 7. Dissolution profiles of insulin 3D printed cone and pyramid shaped microneedles.

4. Conclusions

A 3D printing stereolithographic technique was introduced for the fabrication of microneedle designs for insulin transdermal delivery. SLA facilitated the printing of high quality MNs with various designs. Insulin formulations with mannitol, trehalose and xylitol were deposited on the MN surface using inkjet printing to provide accurate and reproducible active coating layers. All carriers were found to preserve insulin integrity, namely the α-helix and β-Sheet, with xylitol presenting the foremost performance. Franz cell diffusion studies revealed rapid insulin release rates within 30 min. In conclusion, it has been demonstrated that 3D printing can be efficiently used for the fabrication of microneedles for TDD.

Acknowledgments

The authors would like to thank the Coordenação de Aperfeiçoamento de Pessoal de Nível Superior (CAPES) Foundation – Ministry of Education of Brazil.

References

Alkilani, A.Z., McCrudden, M.T.C., Donnelly, R.F., 2015. Transdermal drug delivery: innovative pharmaceutical developments based on disruption of the barrier properties of the stratum corneum. Pharmaceutics 7, 438–470.
Andrade, F., Fonte, P., Oliva, M., Videira, M., Ferreira, D., Sarmento, B., 2015. Solid state formulations composed by amphiphilic polymers for delivery of proteins: Characterization and stability. Int. J. Pharm. 486, 195–206.
Carpenter, J.F., Crowe, J.H., 1989. An infrared spectroscopic study of the interactions of carbohydrates with dried proteins. Biochemistry 28 (9), 3916–3922.
Chen, W., Li, H., Shi, D., Liu, Z., Yuan, W., 2016. Microneedles as a delivery system for gene therapy. Front. Pharmacol. 7, 137.
Davis, S.P., Landis, B.J., Adams, Z.H., Allen, M.G., Prausnitz, M.R., 2004. Insertion of microneedles into skin: measurement and prediction of insertion force and needle fracture force. J. Biomech. 37, 1155–1163.
Dillon, C., Hughes, H., O'Reilly, N.J., McLoughlin, P., 2017. Formulation and characterisation of dissolving microneedles for the transdermal delivery of therapeutic peptides. Int. J. Pharm. 526, 125–136.
Economidou, S.N., Lamprou, D.A., Douroumis, D., 2018. 3D printing applications for transdermal drug delivery (. Int. J. Pharm in press).
Ettinger, M.J., Timasheff, S.N., 1971. Optical activity of insulin. II. Effect of nonaqueous solvents. Biochemistry 10 (5), 831–840.
Gittard, S.D., Chen, B., Xu, H., Ovsianikov, A., Chichkov, B.N., Monteiro-Riviere, N.A., Narayan, R.J., 2013. The effects of geometry on skin penetration and failure of polymer microneedles. J. Adhes. Sci. Technol. 27, 227–243.

Gittard, S.D., Miller, P.R., Jin, C., Martin, T.N., Boehm, R.D., Chisholm, B.J., Stafslien, S.J., Daniels, J.W., Cilz, N., Monteiro-Riviere, N.A., Nasir, A., Narayan, R.J., 2011. Deposition of antimicrobial coatings on microstereolithography-fabricated microneedles. JOM 63, 59–68.

Guo, X., Wang, W., 2017. Challenges and recent advances in the subcutaneous delivery of insulin. Expert Opin. Drug Deliv. 14 (6), 727–734.

Hull, C.W., 1984. Apparatus for production of three-dimensional objects by stereolithography. US 4575330 A.

Ita, K., 2015. Transdermal delivery of drugs with microneedles-Potential and challenges. Pharmaceutics 7, 90–105.

Kaushik, S., Hord, A.H., Denson, D.D., McAllister, D.V., Smitra, S., Allen, M.G., Prausnitz, M.R., 2001. Lack of pain associated with microfabricated microneedles. Anesth. Analg. 92, 502–504.

Kim, Y.C., Park, J.H., Prausnitz, M.R., 2012. Microneedles for drug and vaccine delivery. Adv. Drug Deliv. Rev. 64 (14), 1547–1568.

Kim, Y.H., Sioutas, C., Shing, K.S., 2009. Influence of stabilizers on the physicochemical characteristics of inhaled insulin powders produced by supercritical antisolvent process. Pharm. Res. 26 (1), 61–71.

Kodama, H., 1981. A scheme for three-dimensional display by automatic fabrication of three-dimensional model. IEICE Trans. Electron. J64, 237.

Lu, Y., Mantha, S.N., Crowder, D.C., Chinchilla, S., Shah, K.N., Yun, Y.H., Wicker, R.B., Choi, J.-W., 2015. Microstereolithography and characterization of poly(propylene fumarate)-based drug-loaded microneedle arrays. Biofabrication 7 (4), 045001.

McCrudden, M.T.C., Alkilani, A.Z., Courtenay, A.J., McCrudden, C.M., McCloskey, B., Walker, C., Alshraiedeh, N., Lutton, R.E.M., Gilmore, B.F., Woolfson, A.D., Donelly, R.F., 2015. Considerations in the sterile manufacture of polymeric microneedle arrays. Drug Deliv. Transl. Res. 5, 3–14.

McCrudden, M.T.C., Alkilani, A.Z., McCrudden, C.M., McAlister, E., McCarthy, H.O., Woolfson, A.D., Donnelly, R.F., 2014. Design and physicochemical characterisation of novel dissolving polymeric microneedle arrays for transdermal delivery of high dose, low molecular weight drugs. J. Control. Release 180, 71–80.

Melberg, Steen G., Curtis Johnson, W., 1990. Changes in secondary structure follow the dissociation of human insulin hexamers: a circular dichroism study. Proteins Struct. Funct. Bioinf. 8 (3), 280–286.

Moreno, E., Schwartz, J., Calvo, A., Blanco, L., Larrea, E., Irache, J.M., Sanmartín, C., Coulman, S.A., Soto, M., Birchall, J.C., Espuelas, S., 2017. Skin vaccination using microneedles coated with a plasmid DNA cocktail encoding nucleosomal histones of Leishmania spp. Int. J. Pharm. 533, 236–244.

Narayan, R.J., 2014. Transdermal delivery of insulin via microneedles. J. Biomed. Nanotechnol. 10 (9), 2244–2260.

Pailler-Mattei, C., Bec, S., Zahouani, H., 2008. In vivo measurements of the elastic mechanical properties of human skin by indentation tests. Med. Eng. Phys. 30, 599–606.

Pedde, R.D., Mirani, B., Navaei, A., Styan, T., Wong, S., Mehrali, M., Thakur, A., Mohtaram, N.K., Bayati, A., Dolatshahi-Pirouz, A., Nikkhah, M., Willerth, S.M., Akbari, M., 2017. Emerging biofabrication strategies for engineering complex tissue constructs. Adv. Mater. 29, 1–27.

Ross, S., Scoutaris, N., Lamprou, D., Mallinson, D., Douroumis, D., 2015. Inkjet printing of insulin microneedles for transdermal delivery. Drug Deliv. Transl. Res. 5, 451–461.

Sanjay, S.T., Zhou, W., Dou, M., Tavakoli, H., Ma, L., Xu, F., Li, X.J., 2017. Recent advances of controlled drug delivery using microfluidic platforms (. Adv. Drug Deliv. Rev in press).

Sarmento, B.D., Ferreira, C., Jorgensen, L., van de Weert, M., 2007. Probing insulin's secondary structure after entrapment into alginate/chitosan nanoparticles. Eur. J. Pharm. Biopharm. 65 (1), 10–17.

Schiffter, H., Condliffe, J., Vonhoff, S., 2010. Spray-freeze-drying of nanosuspensions: the manufacture of insulin particles for needle-free ballistic powder delivery. J. R. Soc. Interface 7, 483–500.

Sreerama, N., Woody, R.W., 2000. Anal. Biochem. 287, 252–260.

Souillac, P.O., Middaugh, C.R., Rytting, J.H., 2002. Investigation of protein/carbohydrate interactions in the dried state. 2. Diffuse reflectance FTIR studies. Int. J. Pharm. 235 (1–2), 207–218.

Timasheff, S.N., 1993. The control of protein stability and association by weak interactions with water: how do solvents affect these processes? Annu. Rev. Biophys. Biomol. Struct. 22, 67–97.

Uddin, M.J., Scoutaris, N., Klepetsanis, P., Chowdhry, B., Prausnitz, M.R., Douroumis, D., 2015. Inkjet printing of transdermal microneedles for the delivery of anticancer agents. Int. J. Pharm. 494, 593–602.

Wermeling, D.P., Banks, S.L., Hudson, D.A., Gill, H.S., Gupta, J., Prausnitz, M.R., Stinchcomb, A.L., 2008. Microneedles permit transdermal delivery of a skin-impermeant medication to humans. Proc. Natl. Acad. Sci. U.S.A. 105, 2058–2063.

Yao, G., Quan, G., Lin, S., Peng, T., Wang, Q., Ran, H., Chen, H., Zhang, Q., Wang, L., Pan, X., Wu, C., 2017. Novel dissolving microneedles for enhanced transdermal delivery of levonorgestrel: in vitro and in vivo characterization. Int. J. Pharm. 534, 378–386.

Yong, Z., Yingjie, D., Xueli, W., Jinghua, X., Zhengqiang, L., 2009. Conformational and bioactivity analysis of insulin: freeze-drying TBA/water co-solvent system in the presence of surfactant and sugar. Int. J. Pharm. 371, 71–81.

Yu, N.T., Liu, S.C., O'Shea, D.C., 1972. Laser Raman spectroscopy and the conformation and proinsulin of insulin. J. Mol. Biol. 70 (1), 117–132.

Yu, W., Jiang, G., Liu, D., Li, L., Chen, H., Liu, Y., Huang, Q., Tong, Z., Yao, J., Kong, X., 2017a. Fabrication of biodegradable composite microneedles based on calcium sulfate and gelatin for transdermal delivery of insulin. Mater. Sci. Eng. C 71, 725–734.

Yu, W., Jiang, G., Zhang, Y., Liu, D., Xu, B., Zhou, J., 2017b. Polymer microneedles fabricated from alginate and hyaluronate for transdermal delivery of insulin. Mater. Sci. Eng. C 80, 187–196.